Molecular Dynamics Simulation of Crack Propagation in Nanoscale Polycrystal Nickel Based on Different Strain Rates

Yanqiu Zhang and Shuyong Jiang *

College of Mechanical and Electrical Engineering, Harbin Engineering University, Harbin 150001, China;
zhangyq@hrbeu.edu.cn
* Correspondence: jiangshuyong@hrbeu.edu.cn; Tel.: +86-0451-8251-9710

Abstract: Based on the strain rates of 2×10^8 s^{-1} and 2×10^{10} s^{-1}, molecular dynamics simulation was conducted so as to study mechanisms of crack propagation in nanoscale polycrystal nickel. The strain rate has an important effect on the mechanism of crack propagation in nanoscale polycrystal nickel. In the case of a higher strain rate, local non-3D-crystalline atoms are induced and Lomer-Cottrell locks are formed, which plays a critical role in crack initiation and propagation. Orientation difference between adjacent grains leads to the slipping of dislocations along the different directions, which results in the initiation of a void near the triple junction of grain boundaries and further contributes to accelerating the crack propagation.

Keywords: metals; deformation; crack growth; polycrystal; molecular dynamics

1. Introduction

Fracture of engineering materials frequently leads to failure of structures and components and thus this issue has attracted more and more attention in the engineering fields. Continuum mechanics and theory have played a significant role in investigating the mechanisms of fracture of engineering materials. In particular, fracture frequently takes place along with plastic deformation in metal materials. In general, the occurrence of fracture is closely related to the initiation and propagation of cracks or the initiation and growth of voids. In the most common circumstances, the mechanism of crack formation in the ductile metals involves a process of nucleation, growth and coalescence of voids. Therefore, it is of great significance to reveal the mechanism of initiation and propagation of cracks on the basis of several length scales, such as the macroscale, mesoscale, microscale and nanoscale (or atomic scale). So far, based on the aforementioned four scales, many researchers have devoted themselves to revealing the mechanisms of initiation and propagation of cracks by numerical simulation methods which principally include continuum mechanics finite element method (CMFEM), crystal plasticity finite element method (CPFEM), discrete dislocation dynamics (DDD) method and molecular dynamics (MD) method. These simulation methods are suitable for various scales, where each scale can be separately used for analyzing the mechanisms of crack propagation. Furthermore, multiscale modeling and simulation have been applied to investigate the mechanisms of crack propagation. One approach is to deliver information from a lower scale to a higher scale by means of the parameters involved. Another approach is to directly couple the different scales on the basis of a single computation, such as coupling molecular dynamics with continuum plasticity [1], coupling discrete dislocation dynamics with crystal plasticity [2], and coupling molecular dynamics with discrete dislocation dynamics [3].

It is well known that the simulation methods based on different scales play different roles in analyzing the mechanisms of crack propagation. In general, CMFEM is established on the basis of linear

elastic or elastic plastic fracture mechanics. Therefore, the merit of CMFEM is that it is able to resolve the fracture problems at the macroscopic scale, where it can be used to obtain the stress field, the strain field, the size and shape of plastic zone around the crack tip and the stress intensity factor [4,5]. Compared with CMFEM, the main advantage of CPFEM is that it is able to tackle anisotropic micromechanical problems in crystalline materials, where their mechanical effects are dependent on orientation due to the underlying crystalline structure [6,7]. Therefore, CPFEM becomes a powerful candidate for understanding the mechanisms of crack propagation when the crack propagates in a single crystal or in a polycrystal with crystallographic texture [8,9]. Kartal et al. [10] studied the effect of crystallographic orientation on stress state and plasticity at the crack tip in a hexagonal close-packed (HCP) single crystal Ti through CPFEM and they found that the size and shape of the plastic zone at the crack tip is strongly dependent on crystallographic orientation, but the stress state at the crack tip shows little dependence on crystallographic orientation. Sabnis et al. [11] studied the influence of secondary orientation on plastic deformation near the notch tip in a notched Ni-based single crystal by means of CPFEM, where the slip patterns and the size and shape of plastic zone are strongly dependent on the secondary orientation of the notch, which has an important effect on the initiation and propagation of crack. Li et al. [12] predicted the initiation of a fatigue crack in a polycrystalline aluminum alloy by means of CPFEM, where the grain size, grain shape and grain orientation are considered. Lin et al. [13] studied the propagation of a transgranular crack in a polycrystalline nickel-based superalloy by means of CPFEM and they demonstrated that plastic deformation at the crack tip is related to the grain orientation.

Discrete dislocations play a dual role in plastic deformation at a crack tip. On one hand, plastic deformation, which results from the motion of dislocations, enhances the resistance to crack propagation. On the other hand, local stress concentrations induced by organized dislocation structures contribute to crack propagation. Therefore, the advantage of the DDD method is that it is able to simulate the plastic deformation near the crack tip or around the void according to the evolution of discrete dislocations and hence it is capable of capturing the formation of dislocation structures at a microscopic scale [14–16]. In particular, the DDD method has been frequently used to capture the details of discrete dislocation evolution near the crack tip and around the void. So far, the DDD method has been applied from a single crystal material to a polycrystalline material. Segurado and Llorca [17] revealed the micromechanisms of plastic deformation and void growth in an isolated face-centered cubic (FCC) single crystal by means of the DDD method. Liang et al. [18] investigated the interaction between the blunt crack and the void in a single crystal by virtue of the DDD method, and they focused on the crack-tip deformation, the void growth. Huang et al. [19] applied the DDD method to simulating plastic deformation near a transgrannular crack tip under cyclic loading conditions by taking into account both dislocation climb and dislocation-grain boundary in a polycrystalline nickel-based superalloy.

As an atomistic simulation technique, MD simulation plays an important role in describing the atomic behavior during plastic deformation and crack propagation of metal materials under mechanical loading. So far, MD simulation has been extensively applied to studying the basic mechanism of crack propagation in single crystal and bicrystal metal materials. Sung and Chen [20] studied crack propagation in single crystal nickel via MD simulation, where they found that Shockley partial dislocations are initiated at the crack tip, and they then propagate along the close-packed (111) plane until the crystal is fractured. Zhang and Ghosh [21] investigated the deformation mechanisms at the crack tip of single crystal nickel with an embedded crack by means of MD simulation and they proposed that some lattice orientations lead to the emission of dislocation loops, whereas other lattice orientations contribute to the formation of twins. Zhou et al. [22] investigated the intergranular crack propagation behaviors of copper bicrystals with different symmetrical tilt grain boundaries via MD simulation. Shimokawa and Tsuboi [23] studied the atomic-scale mechanism of plasticity at intergranular crack tip of aluminum bicrystal with tilt grain boundary via MD simulation. Zhang et al. [24] investigated the

mechanism for intercrystalline crack propagation at twist boundary of nanoscale bicrystal nickel by means of MD.

To our knowledge, few papers in the literature have reported the mechanisms of crack propagation in the polycrystal metal materials via MD simulation. In the present study, on the basis of MD simulation, we comparatively investigate the mechanisms of crack propagation in nanoscale polycrystal nickel in the case of the different strain rates in order to reveal the effect of strain rate on the initiation and propagation of a crack.

2. Modeling and Methods

2.1. Simulation Model

The MD models for nanoscale polycrystal nickel is established based on the non-periodic boundary conditions, as shown in Figure 1. In the simulation, $[111]$, $[\overline{1}\overline{1}2]$ and $[1\overline{1}0]$ directions were set as x, y and z directions of the Cartesian reference frame, respectively. In addition, twist boundaries were applied in all the grain boundaries. The lattice orientations for the grains are illustrated in Figure 1a. All the models were determined as the dimension of $20 \times 20 \times 5$ unit cells, and a notch with the size of $5 \times 1 \times 5$ unit cells was preset in one grain. The simulation is performed according to the following two steps. Firstly, energy minimization was conducted on the initial configurations by fixing the y-direction boundary. Secondly, a velocity-controlled tensile load was applied on the two ends labeled fixed atoms in Figure 1a, where the strain rates were chosen as 2×10^8 s^{-1} and 2×10^{10} s^{-1}, respectively. All the simulations were performed at 0.01 K in order to eliminate the thermal effects. Figure 1b,c illustrate the configurations before relaxation and after relaxation, respectively.
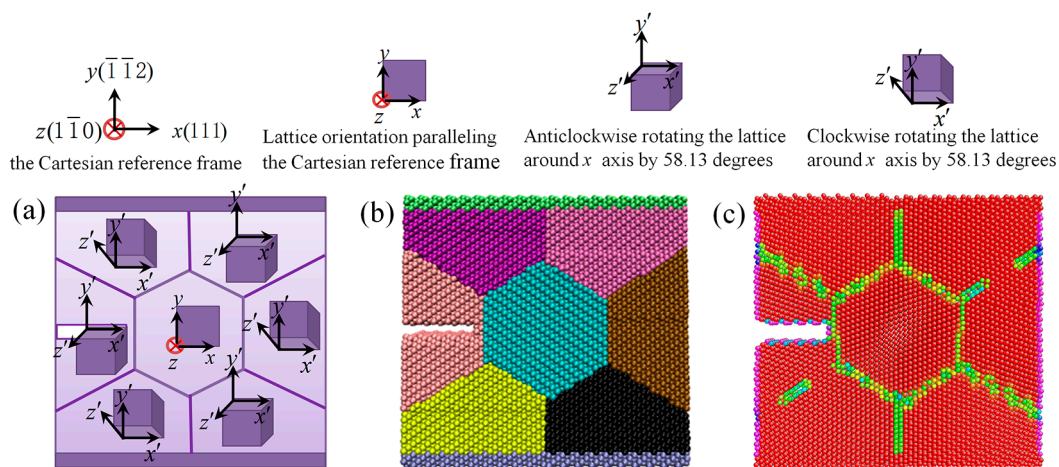
Figure 1. Models for nanoscale polycrystal nickel: (**a**) diagrams of grain orientations; (**b**) configurations before relaxation; (**c**) configurations after relaxation.

2.2. Potential Function

In the current investigation, in order to describe the interactions among nickel atoms, the embedded-atom-method (EAM) potential proposed by Foiles et al. [25] was applied, as expressed in Equation (1).

$$E_{\text{total}} = \sum F_i(\rho_{h,i}) + \frac{1}{2}\sum_i\sum_{j\neq i}\varphi_{ij}(R_{ij}) \tag{1}$$

where E_{total} is the total energy in the system, $\rho_{h,i}$ the host electron density at atom i due to the remaining atoms of the system, $F_i(\rho)$ the energy for embedding atom i into the background electron density ρ, and $\varphi_{ij}(R_{ij})$ the core-core pair repulsion between atoms i and j separated by the distance R_{ij}. In addition,

F_i is related to the element of atom i alone and φ_{ij} is related to the elements of atoms i and j. As stated above, the electron density is approximated by the superposition of atomic densities, namely

$$\rho_{h,i} = \sum_{j \neq i} \rho_j(R_{ij}) \tag{2}$$

where $\rho_j(R_{ij})$ is the electron density supplied by atom j.

2.3. Simulation Methods

In the current investigation, all the simulations were implemented via LAMMPS software [26]. Since only the global mechanical behaviors are considered, Virial stress for an atomic system was used. Lagrangian virial stress has been confirmed to be the most accurate one in terms of evaluating the stress value in dynamical simulations [26].

The centrosymmetry parameter (CSP) was used for analyzing the Shockley partial dislocations as well as stacking faults (SFs), which are induced by tensile deformation. As for the FCC structure, the CSP is defined as follows [27].

$$P = \sum_{i=1,6} \left| \vec{R}_i + \vec{R}_{i+6} \right|^2 \tag{3}$$

where R_i and R_{i+6} are the vectors which correspond to six pairs of opposite nearest neighbors in the FCC lattice. As for atoms in a perfect nickel lattice, the CSP, P, is defined as zero. However, if the nickel lattice is subjected to distortion, the value of P will not be zero. Instead, the specific value of the parameter P will correspond to a particular defect. The dislocation atoms can be observed when all the surface and perfect atoms within the simulation domain are removed.

In order to visualize the defects in the nanoscale nickel crystals, atoms were colored via common neighbor analysis (CNA) [28]. This method is able to detect the environment which an atom is located in, HCP environment or FCC environment. AtomEye [29], a visualization software, was applied for identifying the deformation mechanisms during simulations. In the current investigation, HCP atoms were displayed by light blue color, FCC atoms were expressed by dark blue color and non-3D-crystalline atoms were exhibited by red color. In addition, VMD (Version 1.9.3, Theoretical and Computational Biophysics Group, Urbana, IL, USA, 2016), another visualization software, was also applied to identify the changes in grain boundaries [30].

3. Results and Discussion

Figures 2 and 3 show the process of crack propagation, along with plastic deformation, in nanoscale polycrystal nickel in the case of 2×10^8 s^{-1} and 2×10^{10} s^{-1}, respectively. It can be found from Figures 2 and 3 that in the process of crack propagation, a void begins to occur in the interior of the middle grain. With the progression of plastic deformation, the void gradually grows and finally merges with the initial crack, which contributes to the rapid crack propagation. As a consequence, at the strain of 0.48, the middle grain is subjected to fracture. In the case of high strain rate, in particular, the void tends to be nucleated at trigeminal grain boundaries. In addition, as for different strain rates, the direction in which the void grows exhibits a certain distinction. The phenomenon indicates that the strain rate has an important effect on mechanism of crack propagation in nanoscale polycrystal nickel. It can be generally accepted that the strain rate plays a critical role in the mechanical properties of crystal since it has a predominant influence on the crack propagation. In order to further understand the mechanical properties of nanoscale polycrystal nickel, tensile stress-strain curves are obtained, as shown in Figure 4. It can be seen that purely elastic deformation occurs at early stage of deformation, where the stress increases linearly with increasing strain. When the strain reaches a critical value, the stress drops sharply with increasing strain, which is aroused by the rapid crack propagation. Furthermore, it is evident that the yield stress of nanoscale polycrystal nickel at the strain rate of

2×10^{10} s^{-1} is much higher compared with the one at the strain rate of 2×10^8 s^{-1}, which means that the crack propagation is sensitive to the strain rate.
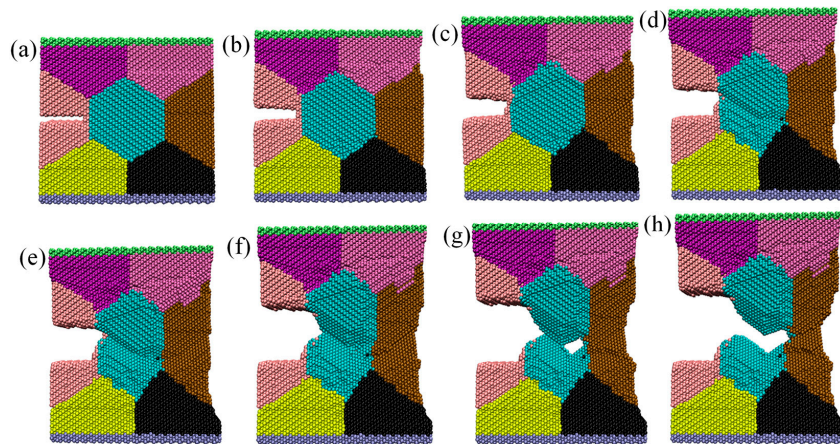
Figure 2. Process of crack propagation in the polycrystal nickel at the strain rate of 2×10^8 s^{-1}: (**a**) $\varepsilon = 0$; (**b**) $\varepsilon = 0.06$; (**c**) $\varepsilon = 0.12$; (**d**) $\varepsilon = 0.18$; (**e**) $\varepsilon = 0.24$; (**f**) $\varepsilon = 0.36$; (**g**) $\varepsilon = 0.42$; (**h**) $\varepsilon = 0.48$.
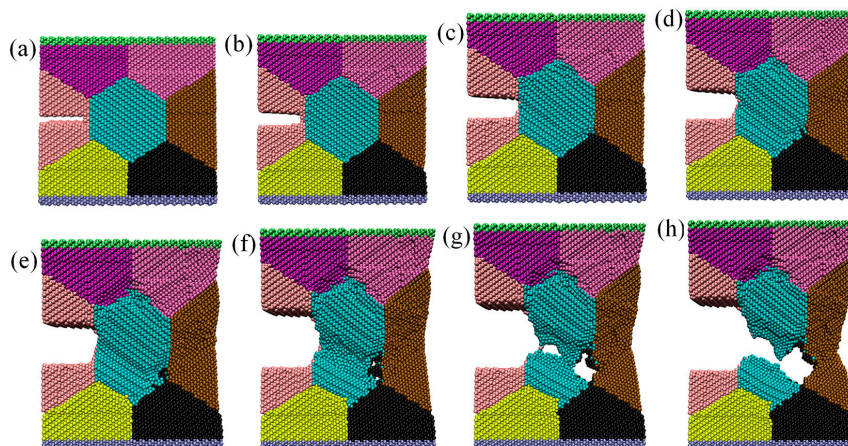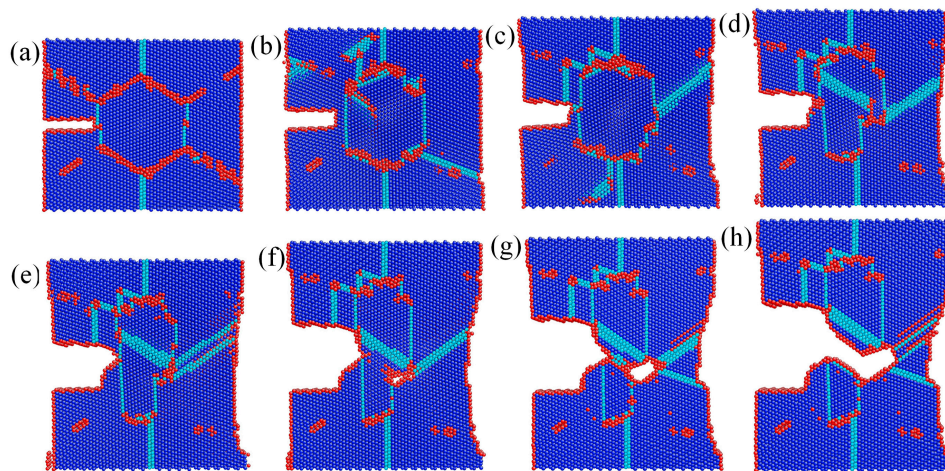

Figure 3. Process of crack propagation in the polycrystal nickel at the strain rate of 2×10^{10} s^{-1}: (**a**) $\varepsilon = 0$; (**b**) $\varepsilon = 0.06$; (**c**) $\varepsilon = 0.12$; (**d**) $\varepsilon = 0.18$; (**e**) $\varepsilon = 0.24$; (**f**) $\varepsilon = 0.36$; (**g**) $\varepsilon = 0.42$; (**h**) $\varepsilon = 0.48$.
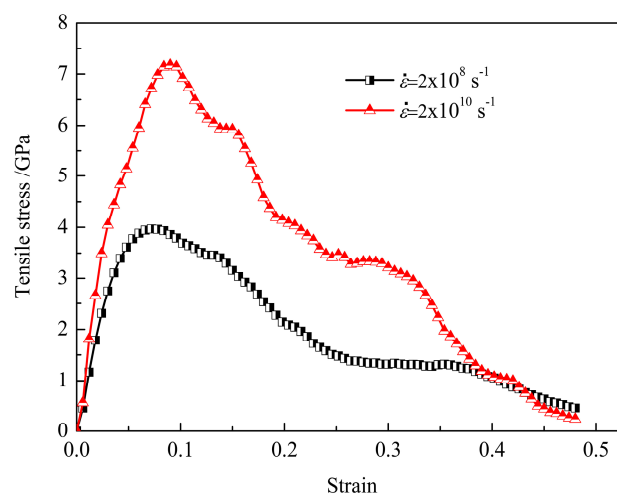

Figure 4. Tensile stress-strain curves for the polycrystal nickel at different strain rates.

For the purpose of further clarifying the process of crack propagation in nanoscale polycrystal nickel, the evolution of the atomic configuration along with crack propagation is captured on the basis of CNA in the case of 2×10^8 s^{-1} and 2×10^{10} s^{-1}, as shown in Figures 5 and 6. It can be found that the dislocations which are emitted from the grain boundaries and the crack tip are capable of moving along the slip plane in the various directions because there is the orientation difference among the grains. In the case of the two strain rates, dislocation slip mainly appears in the middle grain, as well as in the grain which is located to the right of the middle grain. Furthermore, the directions in which the dislocations slip in the two grains exhibit the great discrepancy, which is responsible for the initiation of the void. Compared to 2×10^8 s^{-1}, HCP atoms are distributed in a more complicated way in the nanoscale polycrystal nickel subjected to tensile deformation at the strain rate of 2×10^{10} s^{-1}, where more slip planes are activated.
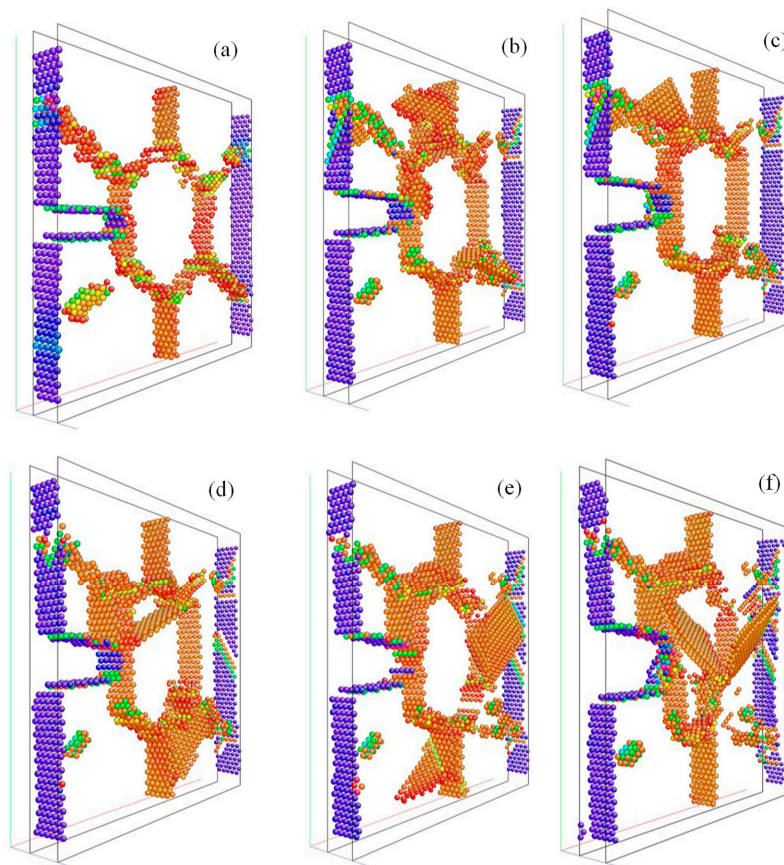

Figure 5. Evolution of atomic configuration for crack propagation in polycrystal nickel at the strain rate of 2×10^8 s^{-1}: (**a**) $\varepsilon = 0$; (**b**) $\varepsilon = 0.06$; (**c**) $\varepsilon = 0.12$; (**d**) $\varepsilon = 0.18$; (**e**) $\varepsilon = 0.24$; (**f**) $\varepsilon = 0.36$; (**g**) $\varepsilon = 0.42$; (**h**) $\varepsilon = 0.48$. (All the configurations are characterized by common neighbor analysis (CNA), where hexagonal close-packed (HCP) atoms were displayed by light blue color, face-centered cubic (FCC) atoms were expressed by dark blue color and non-3D-crystalline atoms were exhibited by red color).
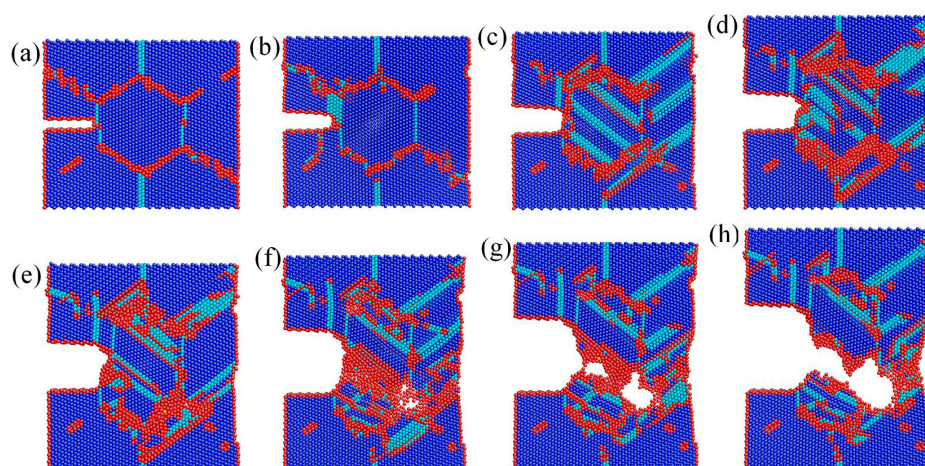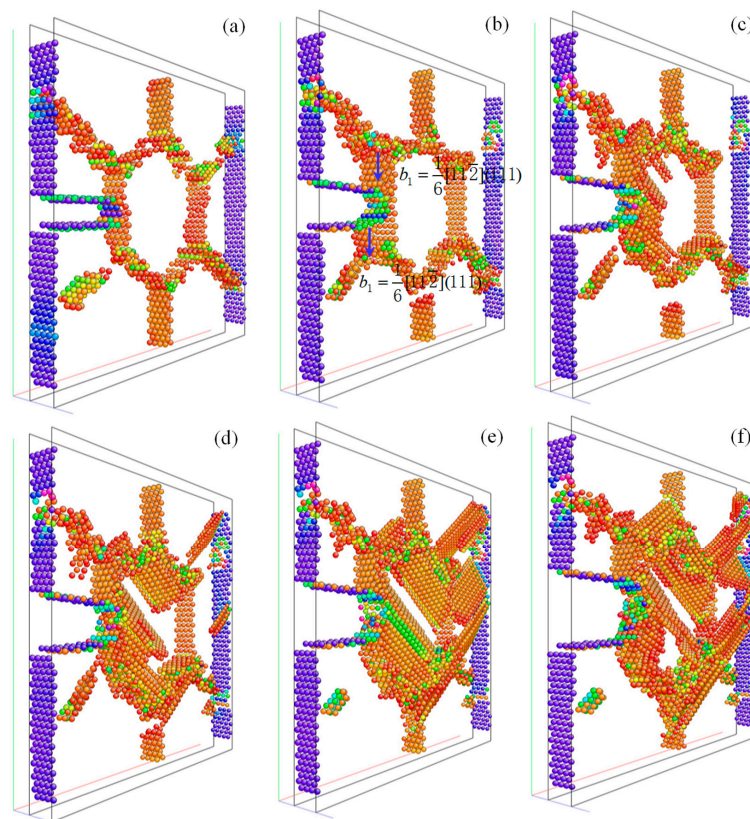

Figure 6. Evolution of atomic configuration for crack propagation in polycrystal nickel at the strain rate of 2×10^{10} s^{-1}: (**a**) $\varepsilon = 0$; (**b**) $\varepsilon = 0.06$; (**c**) $\varepsilon = 0.12$; (**d**) $\varepsilon = 0.18$; (**e**) $\varepsilon = 0.24$; (**f**) $\varepsilon = 0.36$; (**g**) $\varepsilon = 0.42$; (**h**) $\varepsilon = 0.48$. (All the configurations are characterized by CNA, where HCP atoms were displayed by light blue color, FCC atoms were expressed by dark blue color and non-3D-crystalline atoms were exhibited by red color).

For the sake of further clarifying the mechanism of crack propagation in the nanoscale polycrystal nickel, the evolution of the atomic configuration, along with the crack propagation, is captured on the basis of CSP, as shown in Figures 7 and 8. It can be observed from Figure 7 that, with the progression of plastic deformation, Shockley partial dislocations occur along with stacking faults. In particular, at the tensile strain of 0.18, the stacking faults in the adjacent grains are arranged against the grain boundary in the different directions. This phenomenon further indicates that the dislocations in the different grains slip along the different directions in order to accommodate the plastic deformation due to the existence of the grain boundary. It can be seen in Figure 8 that at the early stage of plastic deformation, two Shockley partial dislocations with a Burgers vector $b_1 = 1/6 \, [11\bar{2}] \, (111)$ are initiated from the grain boundary and the crack tip, respectively. Subsequently, increasing Shockley partial dislocations are emitted from the grain boundaries and move along the close-packed {111} planes in the grains. It can be generally accepted that the polycrystal possesses more defects due to the existence of the grain boundaries. As a consequence, more dislocations are emitted from the grain boundaries and then they advance along the various directions due to the orientation difference among the grains.
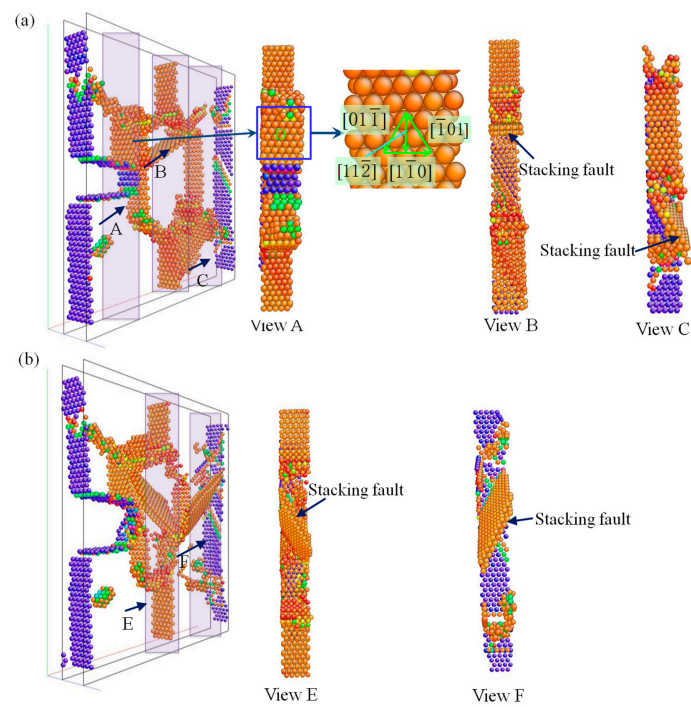

Figure 7. Evolution of atomic configuration in nanoscale polycrystal nickel subjected to early deformation at the strain rate of 2×10^8 s^{-1}: (**a**) $\varepsilon = 0$; (**b**) $\varepsilon = 0.06$; (**c**) $\varepsilon = 0.084$; (**d**) $\varepsilon = 0.096$; (**e**) $\varepsilon = 0.12$; (**f**) $\varepsilon = 0.18$. (All the configurations are characterized by centrosymmetry parameter (CSP), where stacking faults are companied by Shockley partial dislocations).
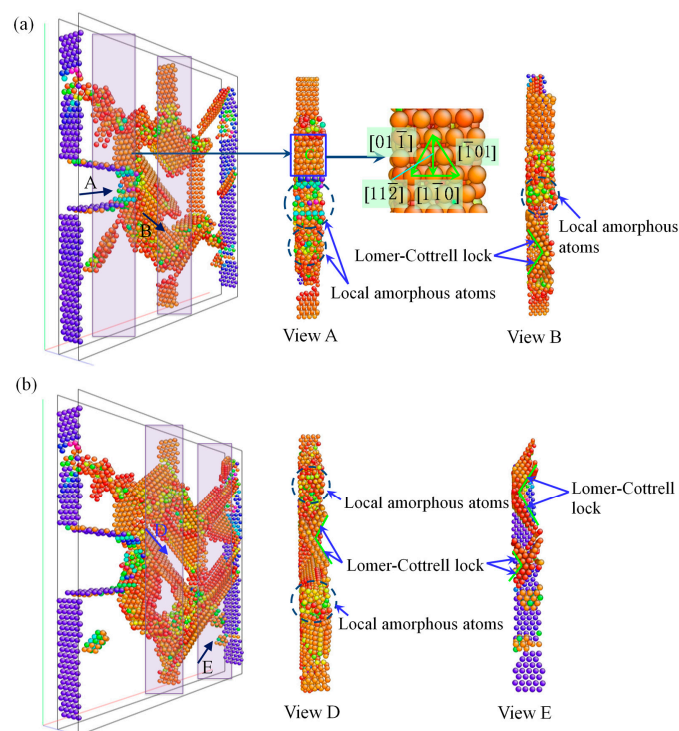
Figure 8. Evolution of atomic configuration in nanoscale polycrystal nickel subjected to early deformation at the strain rate of 2×10^{10} s^{-1}: (**a**) $\varepsilon = 0$; (**b**) $\varepsilon = 0.06$; (**c**) $\varepsilon = 0.084$; (**d**) $\varepsilon = 0.096$; (**e**) $\varepsilon = 0.12$; (**f**) $\varepsilon = 0.18$. (All the configurations are characterized by CSP, where stacking faults are companied by Shockley partial dislocations).

Figures 9 and 10 give a more detailed description of the evolution of the atomic configuration along with crack propagation in the nanoscale polycrystal nickel on the basis of CSP in the case of 2×10^{8} s^{-1} and 2×10^{10} s^{-1}, respectively. It can be found that when the nanoscale polycrystal nickel is subjected to plastic deformation in the case of 2×10^{10} s^{-1}, local non-3D-crystalline atoms are induced and Lomer-Cottrell locks are formed. However, in the case of 2×10^{8} s^{-1}, neither non-3D-crystalline atoms nor Lomer-Cottrell locks are induced, but stacking faults are captured. The phenomena indicate that the mechanisms of crack propagation are different from each other in the case of the two different strain rates. It can be generally accepted that Lomer-Cottrell locks are induced by the interaction between two Shockley partial dislocations which move along the two adjacent {111} slip planes. The Lomer-Cottrell locks are capable of impeding the movement of dislocations, which results in pile-ups of dislocations. As a consequence, the Lomer-Cottrell locks play a critical role in the initiation and propagation of cracks. With the progression of plastic strain, more and more non-3D-crystalline atoms are induced near the Lomer-Cottrell lock. Eventually, the non-3D-crystalline atoms are separated from one another so as to relax the deformation energy, which consequently leads to the initiation and propagation of a crack. Compared to the strain rate of 2×10^{10} s^{-1}, when the nanoscale polycrystal nickel experiences plastic deformation in the case of 2×10^{8} s^{-1}, the less slip systems are activated and consequently Lomer-Cottrell locks are difficult to be formed and simultaneously the non-3D-crystalline atoms are not easy to be induced as well. It can be concluded that in the case of the two strain rates, the initiation of void is more attributed to the fact that the orientation difference between the two adjacent grains leads to the slip of the dislocations along the different directions. Therefore, the occurrence of the void is unavoidable so as to accommodate the compatibility of deformation.

Figure 9. Detailed evolution of atomic configuration in nanoscale polycrystal nickel at the strain rate of 2×10^8 s^{-1}: (**a**) $\varepsilon = 0.096$; (**b**) $\varepsilon = 0.18$. (All the configurations are characterized by CSP, where stacking faults are companied by Shockley partial dislocations).

Figure 10. Detailed evolution of atomic configuration in nanoscale polycrystal nickel at the strain rate of 2×10^{10} s^{-1}: (**a**) $\varepsilon = 0.096$; (**b**) $\varepsilon = 0.18$. (All the configurations are characterized by CSP, where stacking faults are companied by Shockley partial dislocations).

4. Conclusions

Based on the strain rates of 2×10^8 s^{-1} and 2×10^{10} s^{-1}, the mechanisms of crack propagation in nanoscale polycrystal nickel are investigated by means of molecular dynamics simulation. The following conclusions are drawn.

(1) The strain rate has an important effect on mechanisms of crack propagation in nanoscale polycrystal nickel. The yield stress is sensitive to the strain rate, and the yield stress of nanoscale polycrystal nickel at the strain rate of 2×10^{10} s^{-1} is much higher than the counterpart at the strain rate of 2×10^8 s^{-1}.

(2) When the nanoscale polycrystal nickel is subjected to plastic deformation in the case of 2×10^{10} s^{-1}, local non-3D-crystalline atoms are induced and Lomer-Cottrell locks are formed. However, in the case of 2×10^8 s^{-1}, neither non-3D-crystalline atoms nor Lomer-Cottrell locks are induced, but stacking faults are captured.

(3) Lomer-Cottrell locks are able to impede the movement of dislocations and thus lead to the pile-up of dislocations. In addition, the non-3D-crystalline atoms are easy to be induced near the Lomer-Cottrell locks. Consequently, Lomer-Cottrell locks contribute to accelerating the propagation of crack.

(4) The orientation difference between the adjacent grains leads to slipping of dislocations along the different directions, which results in the initiation of a void in the vicinity of the triple junction of grain boundaries. The coalescence of the void with the crack contributes to accelerating the propagation of cracks.

Author Contributions: Yanqiu Zhang, performed MD simulation and wrote the manuscript; Shuyong Jiang, supervised the research.

Conflicts of Interest: The authors declare no conflict of interest.

References

1. Yamakov, V.I.; Warner, D.H.; Zamora, R.J.; Saether, E.; Curtin, W.A.; Glaessgen, E.H. Investigation of crack tip dislocation emission in aluminum using multiscale molecular dynamics simulation and continuum modeling. *J. Mech. Phys. Solids* **2014**, *65*, 35–53. [CrossRef]
2. Cui, Y.; Liu, Z.; Zhuang, Z. Quantitative investigations on dislocation based discrete-continuous model of crystal plasticity at submicron scale. *Int. J. Plasticity* **2015**, *65*, 54–72. [CrossRef]
3. Shilkrot, L.; Miller, R.; Curtin, W.A. Multiscale plasticity modeling: Coupled atomistics and discrete dislocation mechanics. *J. Mech. Phys. Solids* **2004**, *52*, 755–787. [CrossRef]
4. Han, Q.; Wang, Y.; Yin, Y.; Wang, D. Determination of stress intensity factor for mode I fatigue crack based on finite element analysis. *Eng. Fract. Mech.* **2015**, *138*, 118–126. [CrossRef]
5. Benz, C.; Sander, M. Reconsiderations of fatigue crack growth at negative stress ratios: Finite element analyses. *Eng. Fract. Mech.* **2015**, *145*, 98–114. [CrossRef]
6. Ghosh, S.; Anahid, M. Homogenized constitutive and fatigue nucleation models from crystal plasticity FE simulations of Ti alloys, Part 1: Macroscopic anisotropic yield function. *Int. J. Plasticity* **2013**, *47*, 182–201. [CrossRef]
7. Ghosh, S.; Anahid, M. Homogenized constitutive and fatigue nucleation models from crystal plasticity FE simulations of Ti alloys, Part 2: Macroscopic probabilistic crack nucleation model. *Int. J. Plasticity* **2013**, *48*, 111–124.
8. Proudhon, H.; Li, J.; Wang, F.; Roos, A.; Chiaruttini, V.; Forest, S. 3D simulation of short fatigue crack propagation by finite element crystal plasticity and remeshing. *Int. J. Fatigue* **2016**, *82*, 238–246. [CrossRef]
9. Li, J.; Proudhon, H.; Roos, A.; Chiaruttini, V.; Forest, S. Crystal plasticity finite element simulation of crack growth in single crystals. *Comp. Mater. Sci.* **2014**, *94*, 191–197. [CrossRef]

10. Kartal, M.E.; Cuddihy, M.A.; Dunne, F.P.E. Effects of crystallographic orientation and grain morphology on crack tip stress state and plasticity. *Int. J. Fatigue* **2014**, *61*, 46–58. [CrossRef]

11. Sabnis, P.A.; Mazière, M.; Forest, S.; Arakere, N.K.; Ebrahimi, F. Effect of secondary orientation on notch-tip plasticity in superalloy single crystals. *Int. J. Plasticity* **2012**, *28*, 102–123. [CrossRef]

12. Li, L.; Shen, L.; Proust, G. Fatigue crack initiation life prediction for aluminium alloy 7075 using crystal plasticity finite element simulations. *Mech. Mater.* **2015**, *81*, 84–93. [CrossRef]

13. Lin, B.; Zhao, L.G.; Tong, J. A crystal plasticity study of cyclic constitutive behaviour, crack-tip deformation and crack-growth path for a polycrystalline nickel-based superalloy. *Eng. Fract. Mech.* **2011**, *78*, 2174–2192. [CrossRef]

14. Huang, M.; Zhao, L.; Tong, J.; Li, Z. Discrete dislocation dynamics modelling of mechanical deformation of nickel-based single crystal superalloys. *Int. J. Plasticity* **2012**, *28*, 141–158. [CrossRef]

15. Quek, S.S.; Wu, Z.; Zhang, Y.W.; Srolovitz, D.J. Polycrystal deformation in a discrete dislocation dynamics framework. *Acta. Mater.* **2014**, *75*, 92–105. [CrossRef]

16. Fan, H.; Aubry, S.; Arsenlis, A.; El-Awady, J.A. The role of twinning deformation on the hardening response of polycrystalline magnesium from discrete dislocation dynamics simulation. *Acta Mater.* **2015**, *92*, 126–139. [CrossRef]

17. Segurado, J.; Llorca, J. Dsicrete dislocation dynamics analysis of the effect of lattice orientation on void growth in single crystals. *Int. J. Plasticity* **2010**, *26*, 806–819. [CrossRef]

18. Liang, S.; Huang, M.; Li, Z. Discrete dislocation modeling on interaction between type-I blunt crack and cylindrical void in single crystals. *Int. J. Solids Struct.* **2015**, *56–57*, 209–219. [CrossRef]

19. Huang, M.; Tong, J.; Li, Z. A study of fatigue crack tip characteristics using discrete dislocation dynamics. *Int. J. Plasticity* **2014**, *54*, 229–246. [CrossRef]

20. Sung, P.H.; Chen, T.C. Studies of crack growth and propagation of single-crystal nickel by molecular dynamics. *Comp. Mater. Sci.* **2015**, *102*, 151–158. [CrossRef]

21. Zhang, J.; Ghosh, S. Molecular dynamics based study and characterization of deformation mechanisms near a crack in a crystalline material. *J. Mech. Phys. Solids* **2013**, *61*, 1670–1690. [CrossRef]

22. Zhou, Y.; Yang, Z.; Lu, Z. Dynamic crack propagation in copper bicrystals grain boundary by atomistic simulation. *Mater. Sci. Eng. A* **2014**, *599*, 116–124. [CrossRef]

23. Shimokawaa, T.; Tsuboi, M. Atomic-scale intergranular crack-tip plasticity in tilt grain boundaries acting as an effective dislocation source. *Acta Mater.* **2015**, *87*, 233–247. [CrossRef]

24. Zhang, Y.; Jiang, S.; Zhu, X.; Zhao, Y. A molecular dynamics study of intercrystalline crack propagation in nano-nickel bicrystal films with (0 1 0) twist boundary. *Eng. Fract. Mech.* **2016**, *168*, 147–159. [CrossRef]

25. Foiles, S.M.; Baskes, M.I.; Daw, M.S. Embedded-atom-method functions for the FCC metals Cu, Ag, Au, Ni, Pd, Pt, and their alloys. *Phys. Rev. B* **1986**, *33*, 7983–7991. [CrossRef]

26. Plimpton, S.; Parallel, F. Fast parallel algorithms for short-range molecular dynamics. *J. Comput. Phys.* **1995**, *117*, 1–19. [CrossRef]

27. Kelchner, C.L.; Plimpton, S.J.; Hamilton, J.C. Dislocation nucleation and defect structure during surface indentation. *Phys. Rev. B* **1998**. [CrossRef]

28. Tsuzuki, H.; Branicio, P.S.; Rino, J.P. Structural characterization of deformed crystals by analysis of common atomic neighborhood. *Comput. Phys. Commun.* **2007**, *177*, 518–523. [CrossRef]

29. Li, J. AtomEye: An efficient atomistic configuration viewer. *Model. Simul. Mater. Sci. Eng.* **2003**, *11*, 173–177. [CrossRef]

30. Humphrey, W.; Dalke, A.; Schulten, K. VMD-Visual Molecular Dynamics. *J. Mol. Graph.* **1996**, *14*, 33–38. [CrossRef]